Journal of Power Sources 239 (2013) 670–679

Contents lists available at SciVerse ScienceDirect

Journal of Power Sources

journal homepage: www.elsevier.com/locate/jpowsour

Understanding the impedance spectrum of 18650 $LiFePO_4$-cells

J. Illig [a,*], J.P. Schmidt [a], M. Weiss [a], A. Weber [a], E. Ivers-Tiffée [a,b]

[a] Institut für Werkstoffe der Elektrotechnik (IWE), Karlsruhe Institute of Technology (KIT), D-76131 Karlsruhe, Germany
[b] DFG Center for Functional Nanostructures (CFN), Karlsruhe Institute of Technology (KIT), D-76131 Karlsruhe, Germany

HIGHLIGHTS

- Comprehensive impedance analysis of 18650 cell providing a physical interpretation.
- A frequency range from μHz to kHz is covered by combining two measurement methods.
- Use of a reference electrode design to separate electrode contributions.
- Application of the DRT for the investigation of individual frequency ranges.

ARTICLE INFO

Article history:
Received 14 September 2012
Received in revised form
14 November 2012
Accepted 1 December 2012
Available online 12 December 2012

Keywords:
Lithium ion battery
18650
Impedance
Time domain measurement
Reference electrode
DRT

ABSTRACT

The complex nature of lithium ion batteries makes the tracking of individual physical processes difficult. However, having a good knowledge thereof is indispensable for a continuous improvement of cell performance and lifetime.

In this study, the impedance response of a commercial 18650 cell was investigated within a wide frequency range (100 kHz–2 μHz) by combining electrochemical impedance spectroscopy and time domain measurements. In parallel, the original 18650 cell was opened. Thus, the electrode materials could be tested in an experimental test set-up using a reference electrode, which allowed the separation of anode and cathode processes. The different kinds of impedance data sets were de-convoluted in the space of relaxation times, enabling a refined separation of physical processes like charge transfer or solid state diffusion. This multistep approach, which is not tied to a particular electrochemistry, allowed the identification of the dominating physical processes being hidden in the impedance spectrum of the original 18650 cell.

1. Introduction

Lithium ion batteries receive growing attention because of their potentially high energy and power density, which are required for “Electric Vehicles” (EV) and “Hybrid Electric Vehicles” (HEV).

However, material chemistry and fabrication technology of previous cell generations must be improved considerably for application in electric mobility. This task requires characterization methods which are capable to assign performance characteristics to distinctive cell components.

The relevant loss processes in lithium ion cells as well as in alternative cell chemistries occur in a wide frequency range from μHz to MHz frequencies [1]. For instance, the solid state diffusion in the electrodes’ active material is a very slow loss process occurring at frequencies between μHz and Hz frequencies. These frequencies can be investigated adequately by pulse measurements which belong to the group of time domain measurements (TDM). Hereby, the system response of lithium ion cells is evaluated by Fourier transform in order to derive the low frequency impedance spectrum from current pulses [2]. For very high frequencies above 5 kHz, contact resistances between electrode and current collector or between the active material particles contribute to the impedance response. These frequencies are primarily analyzed by electrochemical impedance spectroscopy (EIS) [3], which is also used to analyze the medium frequencies. For these frequencies between 1 Hz and 5 kHz, losses as charge transfer or solid electrolyte interphase (SEI) are dominating the impedance contributions.

Abbreviations: DRT, distribution of relaxation times; EC, ethylene carbonate; ECM, equivalent circuit model; EIS, electrochemical impedance spectroscopy; EMC, ethyl-methyl-carbonate; EV, electric vehicle; FIB, focused ion beam; HEV, hybrid electric vehicle; KK, Kramers Kronig; SEI, solid electrolyte interphase; SEM, scanning electron microscope; SOC, state of charge; TDM, time domain measurement; VC, vinylene carbonate.

* Corresponding author. Tel.: +49 721 60 84 77 14; fax: +49 72160847492.
E-mail address: joerg.illig@kit.edu (J. Illig).

0378-7753/$ – see front matter © 2012 Elsevier B.V. All rights reserved.
http://dx.doi.org/10.1016/j.jpowsour.2012.12.020

A combination of both methods, EIS and TDM, was recently introduced for the characterization of lithium ion cells by our group [2] and is applied in this contribution.

However, the individual time constants of different loss processes are often close to each other and therefore prevent the separation of more than two polarization processes by analyzing the Nyquist plot.

It was already shown in previous papers for solid oxide fuel cells [4–6], that it is advantageous to de-convolute the impedance data in the space of relaxation times. This approach, called DRT (distribution of relaxation times) method, enables a refined separation of physical processes like charge transfer or diffusion losses. Thereby, every physical process is represented as local maximum in a continuous distribution function. The advantages of the DRT method are not tied to a particular electrochemistry.

Recently, it was applied for the first time to lithium ion experimental cells [7–9]. Applying this procedure, cathode and anode polarization processes with close time constants were separated individually and a physically motivated equivalent circuit model (ECM) was established without any a priori settings for the electrochemical system. The loss processes for the investigated lab scale $LiFePO_4$ cathodes have been pegged as: (i) solid state diffusion in the cathode, (ii) charge transfer resistance between cathode and electrolyte, and (iii) contact resistance between cathode and current collector. This allowed for the determination of temperature and SOC-dependency for each individual loss processes. The contact resistance shows no distinctive parameter dependency whereas the other losses show pronounced parameter dependency on both parameters.

An application of this method on commercial cells and its electrodes is desirable in order to understand and afterward improve the current cell generation.

Today, the analysis of commercial cells is usually based on electrochemical impedance spectroscopy at varying operation parameters as state of charge (SOC) or temperature. For the analysis of parameter dependency of loss processes, the Nyquist plots of impedance curves are complemented by the analysis of Bode plots, as the frequency information is not provided in the Nyquist plot visualization [10,11]. The loss processes are usually interpreted by transferring the experience of former investigations or publications to new results [1,10,12]. According to these identified loss processes, which are usually not more than two polarization losses, equivalent circuits are proposed in order to evaluate their parameter dependencies [10,12]. The standard frequency range of these impedance evaluations is limited to 10 kHz for high and 10 mHz for low frequencies.

A more detailed analysis of number and physical origin of loss processes would be profitable in order to understand the reasons for cell performance and aging mechanisms and to avoid the cumulated analysis of several overlapping loss processes.

There are a few publications, using a reference electrode which can be inserted into 18650 cells in order to separate the major contributions of anode and cathode [13,14]. Another way of analysis technique which is introduced in literature is to open the commercial cell and to analyze the single electrodes in experimental cells by reference electrode [15–17] or symmetrical experimental cells [18]. Hereby, an analysis of single electrode contributions to the increase of impedance polarization or to the over voltage is enabled [17,18]. This analysis is usually performed for frequencies between 10 kHz and 10 mHz. The evaluation of smaller frequencies is overlapped by the intercalation capacity which allows only a qualitative evaluation of the real part values. Furthermore, the frequency range is limited as the measurement time increases disproportionately for decreasing frequencies. The analysis of Nyquist plots allows thereby the comparison of the entire polarization of anode and cathode, but not the separate comparison of electrodes losses for individual frequency ranges. The information about time constants of individual loss processes cannot be visualized.

In this study, the impedance response of a commercial 18650 cell is characterized by combining EIS and TDM as shown schematically in Fig. 1. This delivers information over a wide frequency range of 11 decades (2 μHz–100 kHz). Subsequently, the DRT method de-convolutes the impedance spectra in the space of relaxation times in order to analyze the relevant frequency ranges separately. Our aim is to identify the most prominent loss processes which limit performance or lifetime of a commercial 18650 cell. Furthermore, the origin of these processes shall be assigned to anode, cathode, or electrolyte, or interfaces thereof.

For this purpose, a widely used type of 18650 cell ($LiFePO_4$/graphite) is first measured, then opened in a glovebox and the extracted electrodes are re-analyzed in experimental cell set-ups. The contributions of cathode and anode are separated using a reference electrode. Furthermore, the evaluable frequency range is expanded, as impedance spectra of experimental cells are less spoiled by inductive contributions compared to 18650 cells. This allows for a comparative study of measured impedance spectra and the calculated continuous distribution of relaxation times (DRT) of experimental cells with the original 18650 cell.

New insights into the internal loss processes can be given as DRT visualization directly provides information about the characteristic frequencies of loss processes. This allows for an independent evaluation of various frequency ranges and a detailed comparison of experimental and commercial cell measurements via polarization and characteristic frequency of the occurring loss processes.

2. Experimental

2.1. 18650 Cell and its components

In this study we investigate a widely used type of 18650 cell with a nominal capacity of 1.1 Ah. The cell is composed of $LiFePO_4$ and carbon black as cathode and graphite as anode material (Fig. 2). The cathode microstructure shows interesting features in terms of agglomerate size as well as pore size distribution, which was extensively studied by focused ion beam (FIB) tomography in reference [19]. The subsequent characterization in experimental cells necessitates opening of the fully discharged 18650 cell inside a glovebox and extracting anode and cathode sheets thereof. The following procedure is different for anodes and cathodes.

A straightforward extraction is possible for the anode, as some parts of the graphite/copper sheet are coated only on one side with anode material: 1. Punch this part of the anode sheet with an appropriate punching tool, 2. Wash off remaining electrolyte in EMC, 3. Drain off EMC and dry the anode for 10 min in vacuum.

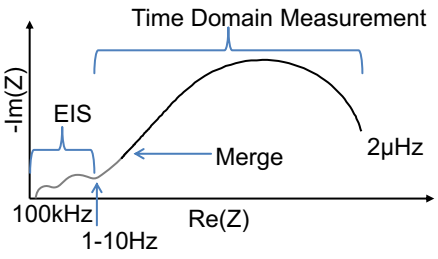

Fig. 1. Schematic for an impedance spectrum ranging from 100 kHz to 2 μHz, which is gained by merging electrochemical impedance spectroscopy for $f \geq 1$ Hz and time domain measurements for $f < 1$ Hz.

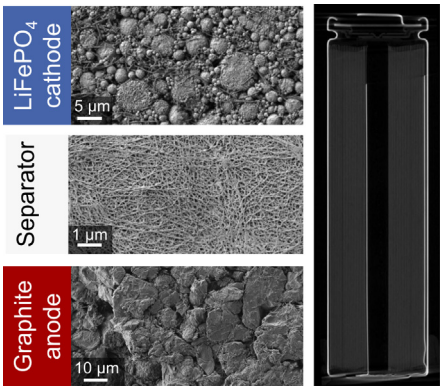

Fig. 2. Left: SEM images of $LiFePO_4$-cathode, separator and graphite anode; right: CT-scan of the 18650 cell.

As the $LiFePO_4$/aluminum sheets are always coated on both sides with cathode material, one coating has to be removed by a dissolving liquid and a cleaning medium. Hence, the preparation of cathodes comprises this additional step. This step also necessitates an extensive drying for at least 3 h at 100 °C in vacuum in order to remove the entire dissolving liquid. Having been prepared this way, anodes and cathodes are stored under glovebox atmosphere and assembled in experimental cells.

2.2. Experimental cells with reference electrode

The experimental cells made of harvested 18650 cell materials are combined in commercially available EL-cell housings [20] with a connection for reference electrodes (ECC-Ref). In this study, all experimental full cells (anode/cathode) are assembled using a reference electrode for electrochemical impedance spectroscopy measurements (Fig. 3), whereas all half cells (anode/lithium metal or cathode/lithium metal) are assembled without reference electrode for time domain measurements. The half cells contain one 1.2 mm thick glass fiber separator whereas the full cells contain four 220 µm glass fiber separators, two on each side of the reference electrode. The electrolyte is based on a EC:EMC 1:1 solvent mixture and contains a 1 M mixture of $LiPF_6$:$LiClO_4$ 1:9 as conducting salt. This mixture is reported to prevent Fe-dissolution from $LiFePO_4$ and to passivate the aluminum current collector [21,22]. Exclusively for time domain measurements, 5% of vinylene carbonate (VC) is added which further improves the cell stability for the extended measurement time [23,24].

The reference electrode used in this study is a V2A steel mesh (195 µm mesh size, 70 µm thickness). This choice was made because a meshed geometry ensures a homogenous current distribution in the liquid electrolyte. This arrangement avoids inductive artifacts or cross talk between anode and cathode, as

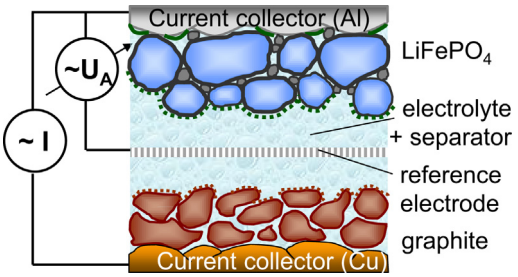

Fig. 3. Set-up of experimental cell for impedance measurements via reference electrode.

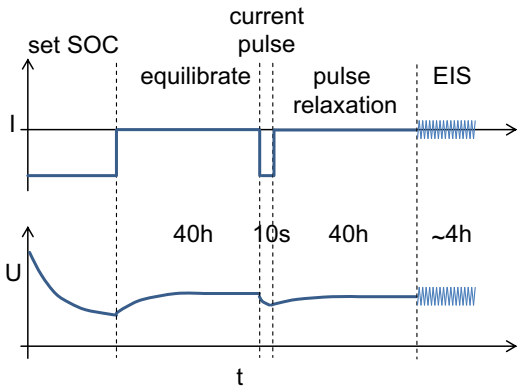

Fig. 4. Measurement procedure of EIS and TDM for 18650 cell at one SOC.

modeled and experimentally verified in [25–27]. However, the reference electrode potential changes slightly at small currents.

2.3. Conducted measurements

All measurements were carried out using a Solartron 1400E cell test system with Scribner Multistat software. For an improved voltage resolution during time domain measurements, additionally an Agilent 34970A and 34901A were used. A standard temperature of 25 °C was adjusted for all measurements and controlled by a Weiss WK1 180 climate test chamber.

2.3.1. 18650 Cell test procedure

1. Stability of the 18650 cell was ensured by 10 times cycling, following a CCCV procedure with a cutoff voltage of 3.6 V and 2.0 V, respectively. Subsequently, the state of charge (SOC) was varied from 90% to 0 % SOC in 10% steps. The SOC is defined by the discharge capacity under standard discharge conditions.
2. Time domain measurements: the 18650 cell was equilibrated before each pulse during a relaxation phase of 40 h. Afterward, the cell was excited by discharge pulses of 1C height and 10 s length. The relaxation phase for the following 40 h was analyzed by Fourier transformation according to [2]. The measurement procedure for one SOC is shown in Fig. 4. The subsequent evaluation of impedance (EIS) and time domain measurements is described in the next chapter.
3. EIS measurements: potentiostatic impedance measurements were conducted for the high and medium frequency domain from 100 kHz to 5 mHz. The voltage amplitude was hereby chosen to be 10 mV (100 kHz–10 Hz) and 5 mV (10 Hz–5 mHz). The impedance measurements were conducted for each SOC after the time domain measurement.

2.3.2. Experimental cell test procedure

1. Stability of experimental cells: the assembled experimental cells were cycled for 20 cycles following a CCCV protocol in order to conduct the formation process. The cutoff voltage for full cells was the same as for the 18650 cells, namely 3.6 V and 2.0 V. For anode half cells it was 0.01 V and 0.8 V whereas the cathode half cells cycled between 2.7 V and 3.7 V. Afterward, impedance and time domain measurements were recorded for varying SOC. The impedance measurements were conducted for full cells with reference electrode whereas the time domain measurements were conducted for full cells without reference electrode and anode and cathode half cells with lithium counter electrode.

2. Time domain measurements (half cells and full cells without reference): time domain measurements were conducted for 80% SOC. Fig. 4 shows the measurement sequence for a time domain measurement. For experimental cells, the discharge pulse was also chosen as 1C/10 s pulse and the voltage relaxation phase was 40 h as well.
3. EIS measurements (full cells with reference): potentiostatic impedance measurements were conducted for the high and medium frequency range from 100 kHz to 10 mHz. The voltage amplitude was hereby chosen to be 10 mV (100 kHz–100 Hz) and 5 mV (100 Hz–10 mHz). The SOC was varied from 100% to 0% SOC in 10% SOC steps.

3. Analysis of EIS and TDM measurement results

3.1. Electrochemical impedance spectroscopy (EIS) measurements

3.1.1. Measurement data quality (Kramers Kronig residuals)

At first, the data quality of our impedance measurements is assessed by calculating the real and the imaginary part of the Kramers Kronig (KK) residuals [28]. Kramers Kronig residuals of a full cell impedance, measured in an experimental cell, are compared to those of the 18650 cell. As Fig. 5 demonstrates, the residuals of both measurements are below 0.3% or even 0.2% within the frequency range from 0.1 Hz to 5 kHz. This data quality is mandatory for a subsequent DRT evaluation. However, the Kramers Kronig residuals increase to 1% for high frequencies $f > 10$ kHz, as the measurement range is changed automatically in the Solartron measurement equipment. This causes a small misalignment in the impedance spectrum which cannot be described by the Kramers Kronig transformation. Furthermore, the inductive tail shows no ideal inductive behavior which also causes increasing residuals.

The Kramers Kronig test is of the greatest importance for impedance measurements between a working electrode and a reference electrode, as this potential is not necessarily stable over time. This instability transgresses the EIS pre-condition of time invariance and limits the validity of measurement results. The influence of potential change is here evaluated by the size of Kramers Kronig residuals which is demonstrated in Fig. 6. Herein, the KK residuals for the full cell impedance are plotted together with the KK residuals for the half cell impedances, i.e., anode and cathode versus reference electrode measurements. As before, KK residuals at high frequencies ($f > 10$ kHz) deviate to higher values caused by the automatically changing measurement range. The KK residuals at medium frequencies (1 Hz $> f >$ 5 kHz) are well below 0.3%, thus proving a very good data quality. However, the KK residuals for measurements via a reference electrode increase significantly to 1% or more for low frequencies ($f < 1$ Hz), which is attributed to the above mentioned instabilities over time. Please recall from chapter 2.3, that pulse measurements were applied on half cells without reference electrode in order to avoid the influence of shifting reference electrode potential.

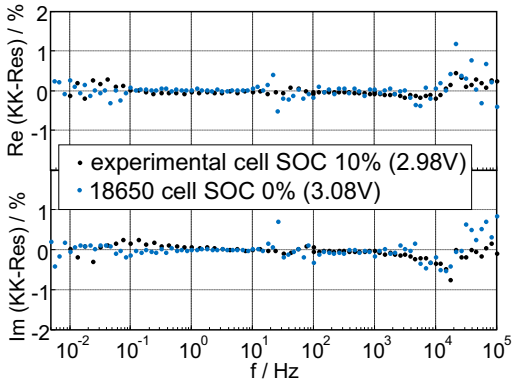

Fig. 5. Real part and imaginary part of Kramers Kronig residuals for experimental full cell (black) and 18650 cell (blue) measurements. (For interpretation of the references to colour in this figure legend, the reader is referred to the web version of this article.)

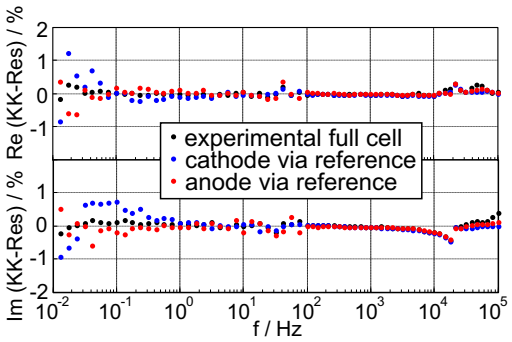

Fig. 6. Real part and imaginary part of Kramers Kronig residuals for experimental full cell (black) and anode (red) and cathode (blue) reference electrode measurements. (For interpretation of the references to colour in this figure legend, the reader is referred to the web version of this article.)

In this study, therefore, EIS measurements are evaluated only in the frequency range 100 kHz $> f >$ 1 Hz. Below these frequencies, impedance data are evaluated only from time domain measurements.

3.1.2. EIS data evaluation by the distribution of relation times (DRT)

In general, EIS is especially useful if the system performance is governed by coupled processes each proceeding at a different rate. However, their number and physical nature are not always identified unambiguously. For electrodes with a complex microstructure, several reaction steps contribute which are hardly separable in the impedance response, as their relaxation frequencies widen out and overlap in the impedance spectrum.

This problem can be avoided, e.g., by the following alternative approach for analyzing impedance spectra. This procedure was developed for the impedance assessment of solid oxide fuel cells and was presented in detail in [4–6]. Recently, it has been applied for the first time for the analysis of experimental lithium ion cells [7–9]. The basic concept of DRT evaluation is described in the next subchapter.

3.1.3. Theory of distribution function of relaxation times (DRT)

The DRT-method uses the fact, that every impedance function that obeys the Kramers–Kronig relations can be represented as an infinite number of infinitesimal small differential RC-elements [3]. This is common in system theory and also holds true for electrochemical systems like lithium ion batteries.

For simplification, Fig. 7a shows the DRT for two ideal processes which can be represented by two RC elements. The RC elements obey the following equation:

$$Z_{\text{complete}} = Z_{RC1} + Z_{RC2} = \frac{R_1}{1 + j\omega R_1 C_1} + \frac{R_2}{1 + j\omega R_2 C_2} = \frac{R_1}{1 + j\omega\tau_1} + \frac{R_2}{1 + j\omega\tau_2} \quad (1)$$

There are two parameters which characterize each RC element and therefore the underlying physical process. The first one is R, giving the polarization of the corresponding process. The second one is the time constant τ, representing the relaxation frequency or rather relaxation time of the process. It is equal to $\tau_i = R_i C_i = (1/2\pi f_i)$.

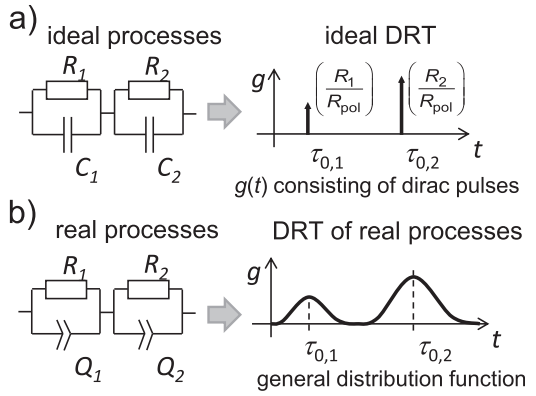

Fig. 7. DRT for a) ideal processes, represented by RC-elements and b) real processes, represented by RQ-elements.

In the given case, the process parameters R and τ can be directly read from the DRT by height and location of the two Dirac peaks. In the following figures, we use the relaxation frequency $f = (1/2\pi\tau)$ instead of the relaxation time τ for the x-values.

Advanced electrodes with a complex microstructure do not have one time constant but a distribution of time constants. An example for such a real system is given in Fig. 7b. Each polarization process is now characterized in the DRT by the center frequency of its peak which is the corresponding relaxation frequency and by the shape of its peak. The area under the peak enclosed to the peak frequency corresponds to the polarization of the loss process. The peak shape of each peak depends on the nature of the underlying process. Some DRT examples for commonly used impedance elements as Warburg element are shown in [5].

3.1.4. DRT calculation

The relation between DRT and impedance curve is given [4] by

$$Z(\omega) = R_0 + Z_{pol}(\omega) = R_0 + R_{Pol} \cdot \int_0^\infty \frac{g(\tau)}{1 + j\omega\tau} \mathrm{d}\tau \tag{2}$$

The term $(g(\tau)/1 + j\omega\tau)\mathrm{d}\tau$ specifies the fraction of the overall polarization with relaxation times between τ and $\tau + d\tau$. R_0 is the ohmic resistance and R_{Pol} the overall polarization. From linear system theory it is well known that the impedance of each entirely capacitive electrical system can be transformed into the form in Eq. (2). However, for a numerical DRT calculation, only a finite number of RC-elements can be used. This finite number of RC-elements can be represented by

$$Z_{pol}(\omega) = \sum_{k=1}^{N} \frac{R_k}{1 + j\omega\tau_k}, \tag{3}$$

giving the overall polarization resistance.

The mathematical problem with the DRT approach arises from the inversion of Eq. (3) which is necessary in order to extract $g(\tau)$ from the measured impedance data $Z_{\mathrm{pol}}(\omega)$. This problem is known to be ill-posed and requires special methods to be solved in order to avoid false peaks and oscillations [4,29,30].

3.2. Time domain measurements (TDM)

For time domain measurements, a pulse signal and the corresponding system response is transformed via Fourier transformation to the frequency domain, and the impedance spectrum is obtained by division of the Fourier coefficients [2]. In this study, we use a current pulse as excitation signal and analyze the system response during and after the excitation.

An ideal current pulse stimulates low frequencies and is therefore adequate to determine an impedance response for several sufficiently low frequencies by one single measurement. The frequency range of a time domain measurement is only restricted by the limited measurement time for low frequencies and the limited sample rate for high frequencies.

The differential capacity ΔC complicates the DRT evaluation of a data set assembled via EIS [8]. However, in TDM it is easily determined by the charge of the current pulse and the voltage gap ΔU before and after the current pulse ΔQ. It is defined as $\Delta C = (\Delta Q/\Delta U)$ and can be directly subtracted from the impedance spectrum measured via TDM.

4. Results and discussion

4.1. Impedance spectra measured by EIS

4.1.1. 18650 Cell

Fig. 8a shows the impedance spectra, measured by EIS only, of the examined 18650 cell for 90% SOC. The impedance is scaled to the electrode area (Ω cm^2), which enables a direct comparison to the impedance spectra of experimental cells presented in chapter 4.1.2.

A capacitive diffusion branch for low frequencies, one flat semicircle for medium frequencies and the typical inductive behavior for high frequencies are immediately observable from the impedance spectrum in Fig. 8a. However, the transformation of these data into the space of relaxation times, shown in Fig. 8b, opens up to details especially in the medium frequency range. Several peaks appear between 1 Hz and 5 kHz which all add up to one single semicircle in the corresponding Nyquist plot. However, frequencies <1 Hz cannot be de-convoluted by DRT without using a pre-processing step, as the DRT calculation requires a convergent impedance curve. Therefore, the subtraction of the capacitive diffusion branch becomes indispensable. The feasibility of this approach was worked out in detail in our recent paper [8].

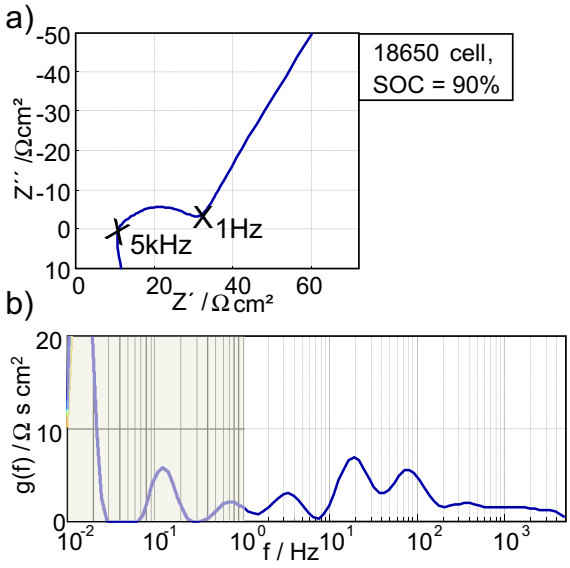

Fig. 8. a) Impedance spectrum (measured by EIS only) and b) distribution of relaxation times (DRT) of 18650 cell for 90% SOC.

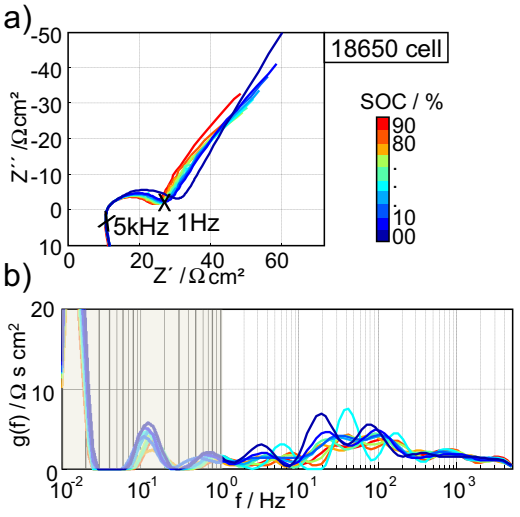

Fig. 9. a) Impedance spectra and b) DRT of 18650 cell for SOC-variation (90%–0%).

In this study, we present a new approach, as the low frequency range will now be investigated by time domain measurements, which works without any pre-processing. For high frequencies, the evaluation is limited by the inductive characteristic of the measured system. The latter overlaps the high frequency loss processes which might occur in the impedance response and prevent an interpretation using the DRT for frequencies above 5 kHz. These frequencies are therefore only analyzed in the experimental cells, as their inductance is much lower.

Furthermore, the 18650 cell is characterized by varying SOC from 90% to 0%, as shown in Fig. 9a. Obviously, its impedance changes not much with SOC, as only for low SOC values the polarization increases slightly. The same conclusion holds for the calculated DRTs, as depicted in Fig. 9b.

4.1.2. Experimental cells with reference electrode

Fig. 10 compares the impedance spectra and DRTs for the experimental full cell at 100% SOC with the impedance measurement and DRT evaluation via reference electrode. The full cell impedance spectrum in Fig. 10a reveals, beside the capacitive diffusion branch for low frequencies and the inductive behavior for frequencies above 100 kHz, two characteristic semicircles. Regarding the impedance curves of anode and cathode via reference electrode in Fig. 10b/c, two semicircles can be assigned to the anodic and one semicircle to the cathodic electrode. The ohmic resistance splits up equally for both electrodes, which indicates an optimal position of the reference electrode. Further, no inductive loops or other typical artifacts can be observed for the impedance measurements via reference electrode [25,26].

Fig. 10 d, e and f show the calculated DRTs in order to give a better separation of anode and cathode contributions. The measured frequencies are divided into three characteristic frequency ranges, denominated as I, II, and III. Frequency range I includes the high frequencies between 5 kHz and 100 kHz. Herein, two characteristic peaks are clearly distinguishable in the calculated DRT of the full cell. The DRTs of anode and cathode are rather similar within this frequency range; therefore both electrodes contribute to the impedance equally. Frequency range II covers frequencies between 10 Hz and 5 kHz. In the DRT, the curve shape of the full cell indicates the existence of up to four characteristic time constants, which is a first hint of either four individual loss processes or less, if a loss process with several coupled time constants takes place here. In this case, an inspection of the reference electrode measurements is supportive again, clearly indicating that the anode dominates the impedance contributions in the entire frequency range II.

Frequency range III, assigned to frequencies below 10 Hz, is only to be analyzed by time domain measurements in Section 4.2. This procedure is required, because EIS impedance data contains a differential capacity, which will cause misleading peaks in the DRT calculation. We have already evaluated this in detail and

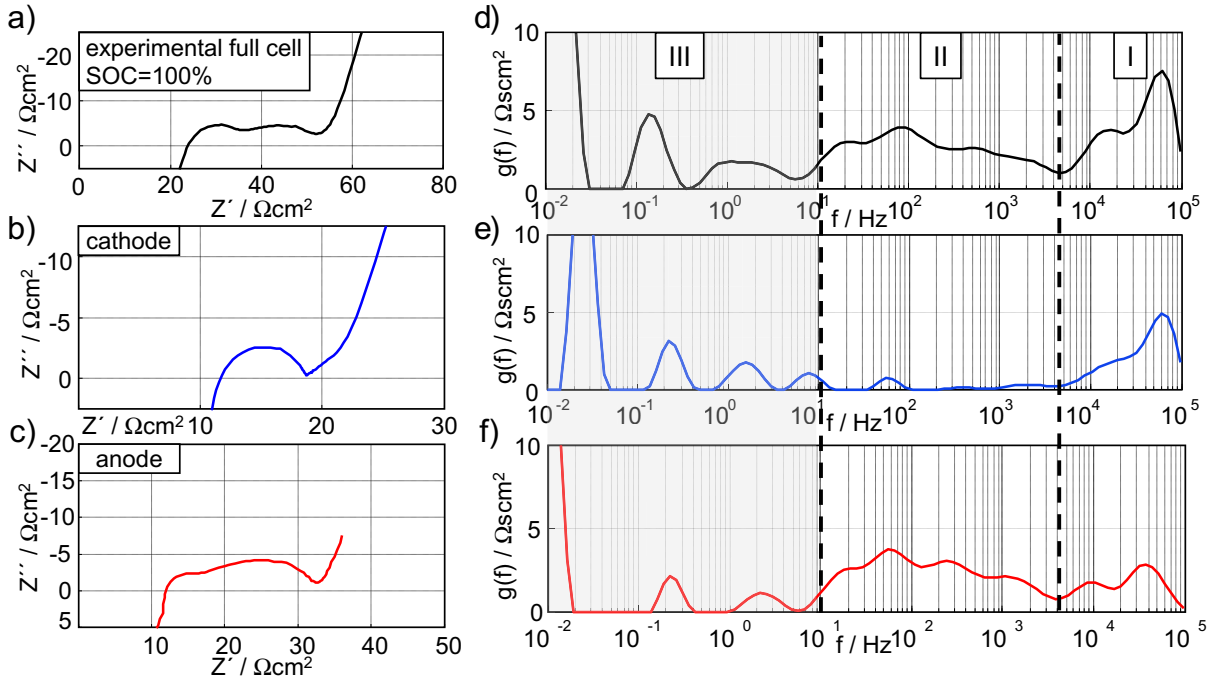

Fig. 10. Left: Impedance spectra measured by EIS of a) an experimental full cell (black), b) cathode (blue) and c) anode (red) determined via reference electrode; right: d), e) and f) calculated corresponding DRTs, all at 100% SOC. (For interpretation of the references to colour in this figure legend, the reader is referred to the web version of this article.)

introduced a pre-processing procedure, as shown in [8], to overcome this problem. Alternatively, as stated in Section 3.2, this frequency range III can be analyzed directly by time domain measurements.

Now we have a look at the SOC variations between 100% and 0% at 25 °C, which are displayed only as DRTs in Fig. 11. First, the DRTs in range II are quite comparable between 18650 cell (Fig. 9) and experimental cell. There are some smaller variations in the shape of the calculated DRTs at SOC >10% within range II, whereas range I remains constant. Noteworthy in range II is the shape of the DRT at SOC = 0%, which corresponds to an open circuit potential of 2.6 V. Here, the predominant peak of the full cell increases significantly in height, changes its shape and its maximum shifts to a more than one order of magnitude lower frequency. The measurements via reference electrode in Fig. 11b/c reveal that this effect is caused exclusively by the anode, whereas the cathode remains unaffected. Please note, that we shifted the lower border of frequency range II from 10 Hz in Fig. 10 to 1 Hz in Fig. 11 in order to include the SOC dependent peak.

4.1.3. Comparison of experimental cell and 18650 cell results (EIS and DRT)

Fig. 12a compares EIS measurements of (i) the 18650 cell (blue solid line) at SOC = 0% (3.08 V) with (ii) the experimental cell (black solid line) at SOC = 10% (2.98 V) and, (iii) the same spectrum of the 18650 cell (blue dotted line), but shifted toward lower frequencies that the capacitive branches of both cells overlap. The corresponding DRTs of both cell types are given in Fig. 12b. A different SOC for both cell types was chosen, because the DRT of the experimental cell steeply increases at SOC = 0% within frequency range II (see Fig. 11), and because open circuit potentials among both cells should be as close as possible.

First of all, the impedance polarization of the experimental cell measurement is in the order of the 18650 cell, when both curves are normalized on the electrode area. However, the shape of the impedance spectra differs noticeably, as for the experimental cell (i) the resistance R_0 is higher, and (ii) the polarization resistance R_{pol} shows two arcs for medium frequencies. These characteristics evolve from the difference in the inductivity of both type of cells. This is concluded from the x-axis interception frequency, which is at 3 kHz for the 18650 cell and at 100 kHz for the experimental cell. Therefore, Fig. 12a also shows a shift of the 18650 cell impedance curve toward higher real part values, until the capacitive branch of both cell types are coincident. This demonstrates that the high frequency part of the 18650 cell impedance is governed by the inductivity of current collectors, which superimposes the polarization losses taking place at the same frequencies. More information is gained from the comparison of both calculated DRTs, displayed in Fig. 12b.

Range I is only accessible by experimental cells with a low inductivity. As already explained in Section 4.1.2, two characteristic peaks are clearly distinguishable, and anode and cathode contribute to the impedance equally. It is deduced, that these high frequency contributions occur as well in the 18650 cell, but they are included in the ohmic resistance R_0 of the 18650 cell. The DRTs in range II, with frequencies correlating to the second semicircle of the impedance spectrum of the experimental cell, show very good agreement in the DRTs. Both type of cells show four peaks located at the same characteristic frequencies. Merely one peak shows different size of polarization. This might result from the electrode preparation procedure or the use of a different electrolyte. As already discussed in Section 4.1.2, the anode dominates the impedance response over the entire frequency range.

Frequency range III, assigned to frequencies lower than 10 Hz, is interpreted only by time domain measurements in Section 4.2.

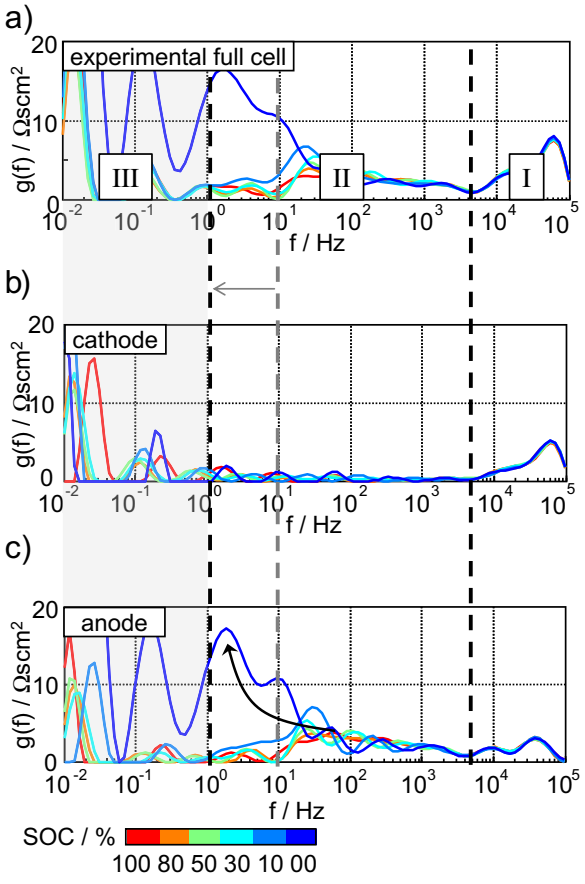

Fig. 11. DRTs calculated from EIS measurements of a) experimental full cell, b) cathode and c) anode measured via reference electrode at SOC-variation.

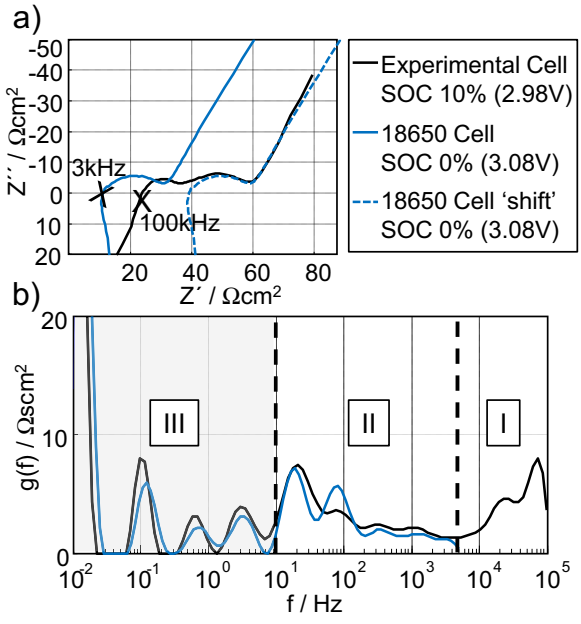

Fig. 12. Comparison of a) EIS measurements of experimental full cell (black) and 18650 cell (blue) and b) corresponding calculated DRTs, both displayed for the 18650 cell at SOC = 0% (3.08 V) and for the experimental cell at SOC = 10% (2.98 V). (For interpretation of the references to colour in this figure legend, the reader is referred to the web version of this article.)

4.2. Impedance spectra measured by TDM

Impedance spectra derived from time domain measurements and the correlated DRTs shown in the following chapter are scaled to the electrode area, which facilitates a comparison of the 18650 cell with the experimental cell. TDM measurements cover the frequencies between 2 μHz and 100 mHz.

4.2.1. 18650 Cell

Fig. 13 shows the current pulse (lower part) with a duration of 10 s, which is put on both cell types as excitation signal (with different current rate) and the voltage response for the 18650 cell (upper part) for a time domain measurement at 80% SOC. The cell voltage decreases during the discharge current pulse. A small part of the relaxation phase is enlarged in order to show the most significant voltage response. Fig. 14 delivers the impedance spectrum as well as the DRT calculated from the time domain response.

The impedance spectrum in this frequency range is composed of one large semicircle, which is much larger than those presented in the previous chapter. The DRT shows a decreasing peak sequence, which is typical for a polarization loss describable by a Warburg element [5]. Furthermore, the DRT reveals one additional large peak at very low frequencies of $f = 2$ μHz which superimposes the Warburg impedance.

4.2.2. Experimental cells without reference electrode

Fig. 15 shows the impedance spectra and the corresponding DRTs of the experimental full cell and the two half cell measurements at 80% SOC and 25 °C. The impedance spectra of full cell and cathode, as for the 18650 cell, are composed of one large semicircle, whereas the anode displays a negligible small contribution in this frequency range. The DRTs of full cell and cathode show a decreasing peak sequence, describable by a Warburg element. It is concluded, that the cathode dominates the impedance contributions in this frequency range.

4.2.3. Comparison of experimental cell and 18650 cell results (TDM)

Now we compare the results compiled by TDM and DRT analysis in Fig. 16. The impedance spectra of the 18650 cell and the experimental cell differ in polarization size and characteristic shape, which holds for the corresponding DRTs as well. Herein, the measured frequency range is now divided in two, range III and range IV. Range III was already previously assigned to the frequencies between 5 μHz and 10 Hz. Herein, the DRTs of experimental cell and 18650 cell are appropriate in polarization magnitude and characteristic

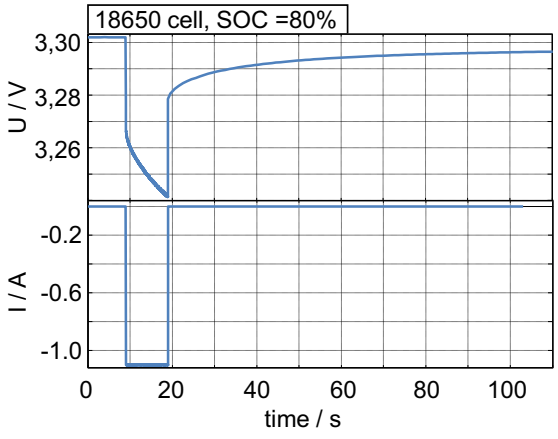

Fig. 13. First part of current step and voltage response for the time domain measurement of an 18650 cell for 80% SOC.

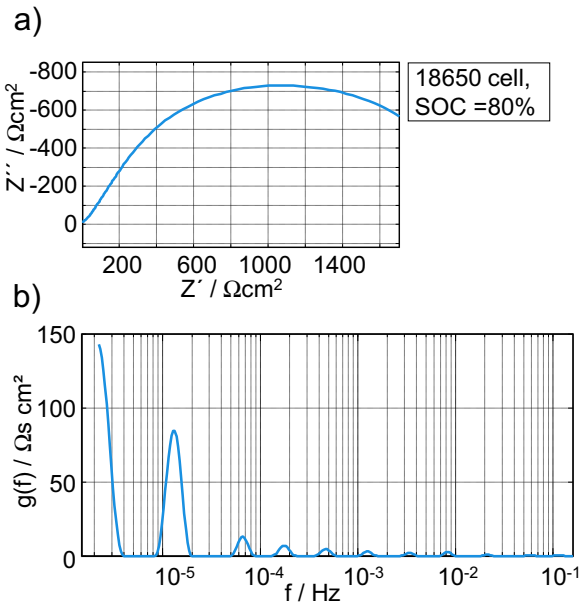

Fig. 14. a) Impedance spectrum measured by TDM and b) corresponding calculated DRT of an 18650 cell at 80% SOC.

frequencies. As already stated in the previous section, these contributions are solely caused by the cathode.

For the newly added range IV, only the DRT of the 18650 cell shows an additional peak near 2 μHz. Thereby, the DRT delivers very helpful information, as this peak explains the difference among both impedance spectra.

4.3. Physical interpretation

As already indicated in Sections 4.1.3 and 4.2.3, the impedances measured by EIS and TDM for an experimental cell are supportive for the physical interpretation of the impedance of an 18650 cell.

4.3.1. Impedance spectra measured by EIS

The resistance value R_0 of the 18650 cell, determined in the high frequency range above 5 kHz (range I), is composed of electrode polarization processes and the ohmic resistance of the electrolyte (Fig. 12). However, the origin of the high frequency processes can be identified easily in experimental cells (Fig. 10). We assume, that the polarization losses at high frequencies originate from the two individual contact resistances between anode/Cu and cathode/Al. This physical interpretation was determined in previous investigations for a $LiFePO_4$-cathode/Al contact resistance [8,31] and is here assumed to be transferable to a graphite-anode/Cu contact resistance. Therefore, the resistance value R_0 of the 18650 is attributed to (i) the two contact resistances between both electrodes and the respective current collector and (ii) the ohmic resistance of the electrolyte.

In the medium frequency range (range II), the impedance curves for experimental cell and 18650 cell are very similar (Fig. 12). This fact allows transferring the conclusions of the measurements via reference electrodes to the 18650 cell. Therefore, the anode dominates the impedance response of the 18650 cell over several frequency decades (10 Hz–5 kHz, Fig. 10). As the DRT reveals anode peaks stretched over 2.5 decades, this indicates a mixed contribution consisting of SEI in combination with charge transfer. Herein, the SOC-variation indicates a strong dependency especially at the lower SOC values for the DRT peak with the slowest time constant (Fig. 11). This DRT peak is therefore assigned to the charge transfer

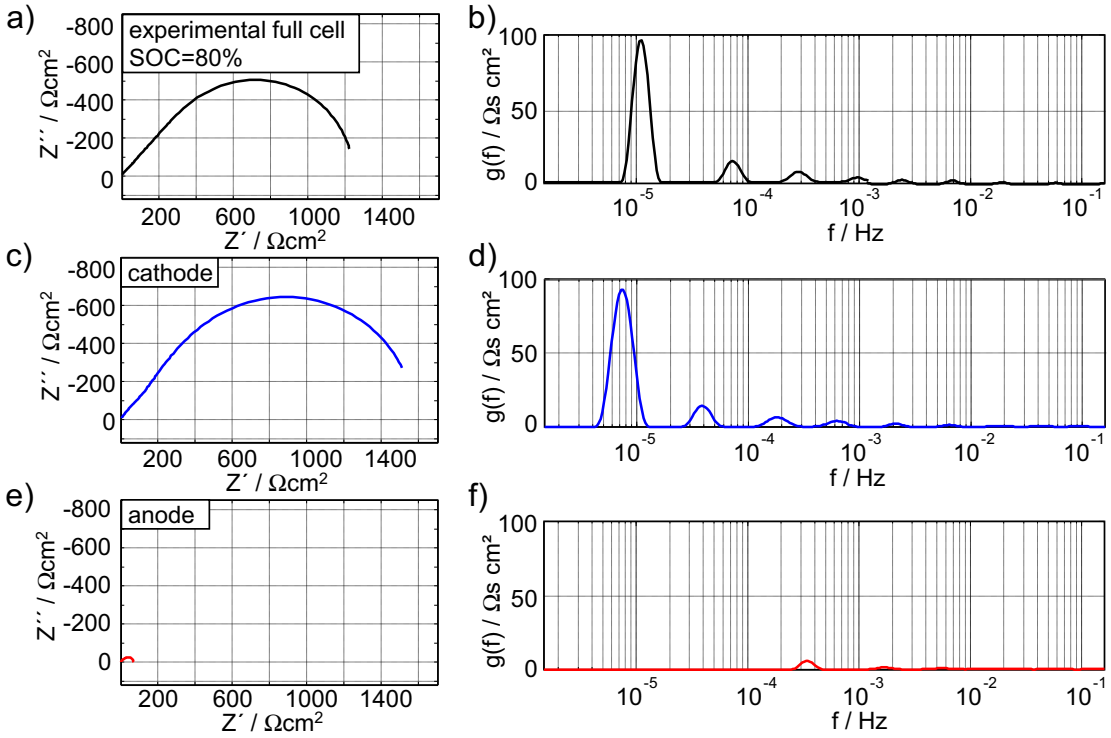

Fig. 15. Left: Impedance spectra measured by TDM and right: corresponding DRTs of (a, b) experimental full cell (black), (c, d) cathode (blue) and (e, f) anode (red) half cells at 80% SOC. (For interpretation of the references to colour in this figure legend, the reader is referred to the web version of this article.)

process anode/electrolyte, whereas the faster, SOC independent peaks are assigned to the SEI layer.

4.3.2. Impedance spectra measured by TDM

The time domain measurements of experimental cells (Fig. 15) point to a Warburg type impedance, which delivers a decreasing peak sequence in the DRT representation [5]. This characteristic points to a solid state diffusion taking place inside the active material. As shown for the experimental cell, the cathode is most relevant for this polarization contribution. Therefore, the solid state diffusion taking place in the $LiFePO_4$ cathode of the 18650 cell is the dominant polarization loss over the entire frequency range III.

Below 5 μHz (range IV), the DRT reveals an additional peak occurring only in the 18650 cell, but not present in the experimental cell (Fig. 16). Hence, this polarization process remains unassignable to anode or cathode, as this DRT peak (a) does not exist in the experimental cell or (b) cannot be measured due to stability problems at these very low frequencies.

Assuming cause (a), the physical origin may be related with a homogenization process inside the entire volume of the electrode layers. Probably, we have uncovered lithium concentration gradients among the electrodes of the 18650 cell. Naturally, such concentration gradients do not exist in the experimental cells having only a very limited electrode area.

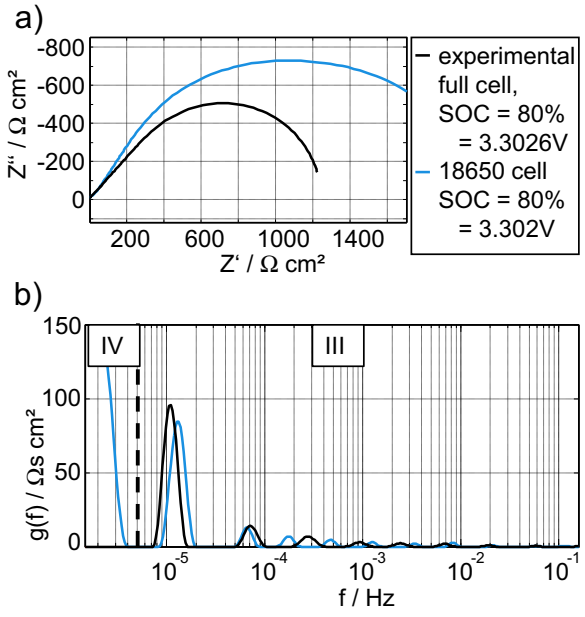

Fig. 16. Comparison of experimental cell (black) and 18650 cell (blue) via a) impedance spectra measured by TDM and b) corresponding calculated DRTs at 80% SOC. (For interpretation of the references to colour in this figure legend, the reader is referred to the web version of this article.)

5. Conclusions

The physical origin of the impedance of a commercial 18650 cell was investigated within a wide frequency range (100 kHz–2 μHz) by combining electrochemical impedance spectroscopy (EIS) and time domain measurements (TDM). In parallel, the original 18650 cell was opened and impedance response of anode and cathode was separated in an experimental test set-up using a reference electrode. Moreover, the different kinds of impedance data sets were de-convoluted in the space of relaxation times (DRT). This multistep approach, which is not tied to a particular electrochemistry, allowed the identification of the dominating physical processes being hidden in the impedance spectrum of the original 18650 cell:

- range I from 100 kHz to 5 kHz (measured by EIS): inductive behavior, most probably originating from the internal current

collectors, dominates the impedance response of the 18650 cell in this frequency range. Experimental cell measurements disclosed that the electrolyte contribution to the ohmic resistance of the 18650 cell is overestimated, as not only the electrolyte as usually assumed [1], but also polarization losses originating from contact resistances anode/Cu and cathode/Al contribute to the "ohmic" resistance, and do not change with SOC.

- range II from 5 kHz to 10 Hz (measured by EIS): the anode dominates the impedance response of the 18650 cell over the entire frequency range. As the DRT de-convolutes several anode peaks with time constants stretched over 2.5 decades, this indicates a mixed contribution of the interface SEI/anode in combination with a charge transfer reaction to the electrolyte. The low frequency peak assigned to charge transfer increases strongly with decreasing SOC.
- range III from 10 Hz to 5 μHz (measured by TDM): the solid state diffusion taking place in the $LiFePO_4$ cathode of the 18650 cell is the dominant polarization loss over the entire frequency range. This is an unexpected result, however, the anode contribution to the polarization loss seems to be negligible small. The portions of cathode and anode show no major changes with SOC.
- range IV at $f < 5$ μHz (measured by TDM): probably, the impedance response of the 18650 cell matching with such a time constant may be related with a homogenization process. It is possible that lithium concentration gradients among the entire volume of the electrodes of the 18650 cell are taking place here. This frequency range was only analyzed for 80% SOC.

Acknowledgements

We gratefully acknowledge the support of our colleagues Moses Ender and Michael Schönleber. This work is funded by the Federal Ministry of Education and Research within the Framework Concept KoLiWIn (fund number03SF0343H) and " Elektrochemie für Elektromobilität – Verbund Süd" (fund number 03KP801) and managed by the Project Management Agency Forschungszentrum Jülich (PTJ). All responsibility for this publication rests with authors.

References

[1] A. Jossen, J. Power Sources 154 (2006) 530–538.
[2] D. Klotz, M. Schönleber, J.P. Schmidt, E. Ivers-Tiffée, Electrochim. Acta 56 (2011) 8763–8769.
[3] J.R. Macdonald, Impedance Spectroscopy, John Wiley & Sons, New York, 1987.
[4] H. Schichlein, A.C. Müller, M. Voigts, A. Krügel, E. Ivers-Tiffée, J. Appl. Electrochem. 32 (2002) 875–882.
[5] A. Leonide, V. Sonn, A. Weber, E. Ivers-Tiffée, J. Electrochem. Soc. 155 (2008) B36–B41.
[6] V. Sonn, A. Leonide, E. Ivers-Tiffée, J. Electrochem. Soc. 155 (2008) B675–B679.
[7] J.P. Schmidt, T. Chrobak, M. Ender, J. Illig, D. Klotz, E. Ivers-Tiffée, J. Power Sources 196 (2010) 5342–5348.
[8] J. Illig, M. Ender, T. Chrobak, J.P. Schmidt, D. Klotz, E. Ivers-Tiffée, J. Electrochem. Soc. 159 (2012) A952–A960.
[9] J. Illig, T. Chrobak, M. Ender, J.P. Schmidt, D. Klotz, E. Ivers-Tiffée, ECS Trans. 28 (2010) 3–17.
[10] D. Andre, M. Meiler, K. Steiner, C. Wimmer, T. Soczka-Guth, D.U. Sauer, J. Power Sources 196 (2011) 5334–5341.
[11] A. Cuadras, O. Kanoun, SoC Li-ion Battery Monitoring with Impedance Spectroscopy, Systems, Signals and Devices, in: SSD '09. 6th International Multi-Conference on, 2009, 2009, pp. 1–5.
[12] P.L. Moss, G. Au, E.J. Plichta, J.P. Zheng, J. Electrochem. Soc. 155 (2008) A986–A994.
[13] G. Nagasubramanian, Impedance Studies on Cathodes in Li-ion Cells, Energy Conversion Engineering Conference and Exhibit, 2000, (IECEC) 35th Intersociety, pp. 968–975.
[14] G. Nagasubramanian, D.H. Doughty, J. Power Sources 150 (2005) 182–186.
[15] D.P. Abraham, J. Liu, C.H. Chen, Y.E. Hyung, M. Stoll, N. Elsen, S. MacLaren, R. Twesten, R. Haasch, E. Sammann, I. Petrov, K. Amine, G. Henriksen, J. Power Sources 119–121 (2003) 511–516.
[16] D.P. Abraham, J.L. Knuth, D.W. Dees, I. Bloom, J.P. Christophersen, J. Power Sources 170 (2007) 465–475.
[17] D.P. Abraham, D.W. Dees, J. Christophersen, C. Ho, A.N. Jansen, Int. J. Energy Res. 34 (2010) 190–203.
[18] K. Amine, C.H. Chen, J. Liu, M. Hammond, A. Jansen, D. Dees, I. Bloom, D. Vissers, G. Henriksen, J. Power Sources 9798 (2001) 684–687.
[19] M. Ender, J. Joos, T. Carraro, E. Ivers-Tiffée, J. Electrochem. Soc. 159 (2012) A972–A980.
[20] www.el-cell.com, el-cell, 29.8.12.
[21] D. Aurbach, B. Markovsky, G. Salitra, E. Markevich, Y. Talyossef, M. Koltypin, L. Nazar, B. Ellis, D. Kovacheva, J. Power Sources 165 (2007) 491–499.
[22] R. Marom, O. Haik, D. Aurbach, I.C. Halalay, J. Electrochem. Soc. 157 (2010) A972–A983.
[23] D. Aurbach, K. Gamolsky, B. Markovsky, Y. Gofer, M. Schmidt, U. Heider, Electrochim. Acta 47 (2002) 1423–1439.
[24] S.S. Zhang, J. Power Sources 162 (2006) 1379–1394.
[25] M. Ender, A. Weber, E. Ivers-Tiffée, J. Electrochem. Soc. 159 (2012) A128–A136.
[26] B.A. Boukamp, Solid State Ionics 143 (2001) 47–55.
[27] S.B. Adler, J. Electrochem. Soc. 149 (2002) E166–E172.
[28] B.A. Boukamp, J. Electrochem. Soc. 142 (1995) 1885.
[29] A.N. Tikhonov, A.V. Goncharsky, V.V. Stepanov, A.G. Yagola, Numerical Methods for the Solution of Ill-Posed Problems, Kluwer Academic Publishers, Dordrecht, Boston, London, 1990.
[30] J. Weese, Comput. Phys. Commun. 69 (1992) 99–111.
[31] M. Gaberscek, J. Moskon, B. Erjavec, R. Dominko, J. Jamnik, Electrochemical Solid State Lett. 11 (2008) A170–A174.